2988 *Chem. Mater.* **2010,** *22,* 2988–2994
DOI:10.1021/cm100393v

CHEMISTRY OF MATERIALS
Article

Design of AgM Bimetallic Alloy Nanostructures (M = Au, Pd, Pt) with Tunable Morphology and Peroxidase-Like Activity

Weiwei He,[†,§] Xiaochun Wu,*[,†] Jianbo Liu,[†,§] Xiaona Hu,[†,§] Ke Zhang,[†,§] Shuai Hou,[†,§] Weiya Zhou,[‡] and Sishen Xie*[,‡]

[†]*CAS Key Laboratory of Standardization and Measurement for Nanotechnology, National Center for Nanoscience and Technology, Beijing 100190, People's Republic of China,* [‡]*National Laboratory for Condensed Matter Physics, Institute of Physics, Chinese Academy of Sciences, Beijing 100190, People's Republic of China, and* [§]*Graduate School of the Chinese Academy of Sciences, Beijing 100190, People's Republic of China*

Received February 8, 2010. Revised Manuscript Received March 26, 2010

Bimetallic alloy nanoparticles (NPs) exhibit unique optical and catalytic properties that are dependent on their morphology and composition. In this paper, a general and facile way was developed to prepare Ag-related bimetallic alloy NPs with hollow/porous structures, including AgAu, AgPd, and AgPt. The formation of the alloy structures is evidenced by high-resolution transmission electron microscopy (TEM), scanning transmission electron microscopy−energy-dispersive X-ray analysis (STEM-EDX) mapping, and ultraviolet−visible−near-infrared (UV−vis−NIR) absorption spectra. AgM alloy NPs exhibit peroxidase-like activity. A unique composition dependence is found and can be used to tailor the catalytic activity. In addition to the recent discoveries about peroxidase mimetics on Fe_3O_4 NPs and sheetlike FeS nanostructures, our findings suggest a new type of candidate as peroxidase mimics. Furthermore, for noble metals, apart from size and shape, tailoring the composition poses another effective way to tune the catalytic activity.

Introduction

Noble-metal nanoparticles (NPs) have received tremendous interest, especially because of their unique optical properties, fascinating catalytic activity, and potential applications in a wide range such as surface plasmonics,[1] biosensor,[2] diagnostics,[3] and catalysis.[4] Their properties are strongly dependent not only on size and shape, but also on composition and structure. Bimetallic nanoalloys have been demonstrated to exhibit improved catalytic performance, because of the synergistic effect and electronic effect.[5] For example, pure Pt nanostructures are readily poisoned by chemisorbed CO-like intermediates generated in the electrochemical oxidation of methanol, which makes their catalytic performance degrade quickly. The formation of bimetallic NPs with other metals, such as Ru,[6] Ag,[7] and Au,[8] can reduce CO poisoning. As a result, to systematically exploit the impact of different bimetallic combinations on properties, it is highly desirable to develop facile and general methods for fabricating alloy nanostructures of a variety of metals. The chemical synthesis of bimetallic alloy NPs can be roughly classified into two approaches. One employs a galvanic replacement reaction.[9] For instance, using Ag nanocubes as a sacrificial template, AuAg, PtAg, and PdAg nanoboxes were obtained. Disadvantages are that the two metals should have a large difference in electrochemical redox potential, which restricts the possible combinations of two metals. In addition, the tunability of alloy composition is limited. We found that by etching Au core/Ag shell (Au@Ag) nanorods (NRs) with Pt ions, $Au@Pt_xAg_{1-x}$ ($0.44 < x < 0.62$) alloy NRs were obtained but with a narrow composition tunabilty.[9f] The other,

*Authors to whom correspondence should be addressed. Phone: +86-10-8254 5577. Fax: +86-10-8254 5577. E-mails: wuxc@nanoctr.cn (X.W.), ssxie@aphy.iphy.ac.cn (S.X.).

(1) (a) Tao, A.; Sinsermsuksakul, P.; Yang, P. D. *Nat. Nanotechnol.* **2007**, *2*, 435. (b) Jain, P. K.; Huang, X. H.; El-Sayed, I. H.; El-Sayed, M. A. *Plasmonics* **2007**, *2*, 107.
(2) Yu, C. X.; Irudayaraj, J. *Anal. Chem.* **2007**, *79*, 572.
(3) Huang, X. H.; El-Sayed, I. H.; Qian, W.; El-Sayed, M. A. *Nano Lett.* **2007**, *7*, 1591.
(4) (a) Schrinner, M.; Ballauff, M.; Talmon, Y.; Kauffmann, Y.; Thun, J.; Möller, M.; Breu, J. *Science* **2009**, *323*, 617. (b) Stamenkovic, V. R.; Fowler, B.; Mun, B. S.; Wang, G.; Ross, P. N.; Lucas, C. A.; Markovic, N. M. *Science* **2007**, *315*, 493. (c) Zhang, J.; Sasaki, K.; Sutter, E.; Adzic, R. R. *Science* **2007**, *315*, 220. (d) Zhao, D.; Xu, B. Q. *Angew. Chem., Int. Ed.* **2006**, *45*, 4955.
(5) (a) Toshima, N.; Yonezawab, T. *New J. Chem.* **1998**, 1179. (b) Ferrando, R.; Jellinek, J.; Johnston, R. L. *Chem. Rev.* **2008**, *108*, 845.
(6) (a) Liu, F.; Lee, J. Y.; Zhou, W. J. *Adv. Funct. Mater.* **2005**, *15*, 1459. (b) Roth, C.; Benker, N.; Theissmann, R.; Nichols, R. J.; Schiffrin, D. J. *Langmuir* **2008**, *24*, 2191.
(7) Zhao, D.; Wang, Y.; Yan, B.; Xu, B. Q. *J. Phys. Chem. C* **2009**, *113*, 1242.
(8) Lou, Y. B.; Maye, M. M.; Han, L.; Luo, J.; Zhong, C. J. *Chem. Commun.* **2001**, 473.
(9) (a) Sun, Y. G.; Xia, Y. N. *Science* **2002**, *298*, 2176. (b) Chen, J. Y.; McLellan, J. M.; Siekkinen, A.; Xiong, Y. J.; Li, Z. Y.; Xia, Y. N. *J. Am. Chem. Soc.* **2006**, *128*, 14776. (c) Chen, J. Y.; Wiley, B.; McLellan, J.; Xiong, Y. J.; Li, Z. Y.; Xia, Y. N. *Nano Lett.* **2005**, *5*, 2058. (d) Sun, Y. G.; Wiley, B.; Li, Z. Y.; Xia, Y. N. *J. Am. Chem. Soc.* **2004**, *126*, 9399. (e) Guo, S. J.; Dong, S. J.; Wang, E. K. *Chem.—Eur. J.* **2008**, *14*, 4689. (f) He, W. W.; Wu, X. C.; Liu, J. B.; Zhang, K.; Chu, W. G.; Feng, L. L.; Hu, X. N.; Zhou, W. Y.; Xie, S. S. *Langmuir* **2010**, *26*, 4443.

Published on Web 04/15/2010

more-popular, approach is based on co-reduction of two metal salts by a strong reductant (such as $NaBH_4$), often with different supplementary means such as dendrimer encapsulation,[10] sol−gel templation,[11] two-phase protocol,[12] or in a sonochemical way.[13] The inconveniences include complex reaction microenvironments and/or tedious cleaning procedures after synthesis. Therefore, simple and facile approaches are still needed for the controlled synthesis of bimetallic NPs with desirable size, shape, and structure (solid or hollow).

Exploitation of new functions of known nanomaterials is one of the most attractive aspects in nanoscience. Recently, Fe_3O_4 magnetic NPs, which are often considered to be biologically and chemically inert, have been discovered with novel peroxidase-like activity.[14a] Afterward, sheetlike FeS nanostructures and spherical CeO_2 NPs were also found with peroxidase- or oxidase-like activity.[14b,c] The new functions make them potentially useful in various biodetections.[14] In addition, small Pt NPs (ca. 5 nm in diameter) were suggested to act as a potent SOD/catalase mimetics, because they could catalyze the decomposition of superoxide free radicals and H_2O_2.[15a] It thus opens the door for their potential application in oxidative stress-related therapeutics such as antiaging, neurodegenerative diseases, and cancers.[15b−d] For instance, the lifespan of *Caenorhabdtis elegans* has been extended by treating with Pt NPs. In comparison with natural enzymes, with the advantages of controlled synthesis in low costs, tunable catalytic activities, and a high stability against stringent reaction conditions, the NPs family may be a promising candidate of enzyme mimetics. Previously, we found that Pt and PtAg alloy NPs showed tunable catalytic activities for AA oxidation by dissolved oxygen.[16] It inspires us to explore: (1) can Pt or other noble-metal NPs be a potential peroxidase or oxidase mimetics? and (2) if so, can the catalytic activity be tailored by forming an alloy with other metals? Considering the limited reports in this new emerging field, further exploration is really deserved.

Because of their excellent optical properties, such as strong surface plasmon resonance (SPR) and huge surface-enhanced Raman scattering (SERS), Ag NPs themselves have received much interest.[17] In contrast, the formation of an alloy nanostructure with other metal is studied relatively rarely. Recently, some reports have demonstrated that alloying with Ag can improve the catalytic activity and optical responses of the other metal.[16,18] Another interesting point is that Ag ions play an important role in the nanocrystal growth for regulating the shape.[19] However, the role of Ag atoms in shape tailoring upon alloying is rarely investigated. Au and Ag have similar lattice constants and are miscible at any alloy composition in bulk. Ag and Pd have a relatively large lattice mismatch (4.9%) and are also miscible in bulk. Ag and Pt have a slightly decreased lattice mismatch (4.2%), in comparison with AgPd combination but with a large miscibility gap in bulk. What type of role do these differences play in the morphology control of the alloy nanostructures?

With aforementioned motivations, we study three types of AgM (M = Au, Pd, and Pt) alloy NPs with an emphasis on the control of shape and structure and the tailoring of catalytic activity. One simple approach is developed to synthesize hollow/porous alloy NPs, based on the co-reduction of Ag and other metal ions by ascorbic acid (AA) in aqueous solutions without any seeds. The morphology of AgM alloy NPs can be tailored by controlling Ag/M ratio and/or surfactant concentration. Similar to horseradish peroxidase (HRP), AgM alloy NPs can quickly catalyze the oxidation of typical HRP substrates in the presence of hydrogen peroxide (H_2O_2). With the example of PdAg alloy NPs, tailoring of peroxidase-like activity is realized by varying alloy composition, which introduces another effective way to regulate the catalytic activity apart from size and shape.

Experimental Section

Chemicals and Reagents. Cetyltrimethylammonium bromide (CTAB), chlorauric acid ($HAuCl_4 \cdot 3H_2O$), potassium(II) tetrachloropalladate (K_2PdCl_4), potassium(II) tetrachloroplatinate (K_2PtCl_4), silver nitrate ($AgNO_3$), L-ascorbic acid (AA), *o*-phenylenediamine (OPD), 3,3′,5,5′-tetramethylbenzidine dihydrochloride (TMB), and 2,2′-azino-bis-(3-ethylbenzo-thiazoline-6-sulfonic acid) diammonium salt (ABTS) were all purchased from Alfa Aesar and used as received. Milli-Q water (18 MΩ cm) was used for all solution preparations. All glassware used in the following procedures was cleaned in a bath of a piranha solution

(10) (a) Wilson, O. M.; Scott, R.W. J.; Martinez, J. C. G.; Crooks, R. M. *J. Am. Chem. Soc.* **2005**, *127*, 1015. (b) Lang, H. F.; Maldonado, S.; Stevenson, K. J.; Chandler, B. D. *J. Am. Chem. Soc.* **2004**, *126*, 12949. (c) Scott, R. W. J.; Wilson, O. M.; Oh, S.; Kenik, E. A.; Crooks, R. M. *J. Am. Chem. Soc.* **2004**, *126*, 15583. (d) Ye, H.; Crooks, R. M. *J. Am. Chem. Soc.* **2007**, *129*, 3627.
(11) Devarajan, S.; Bera, P.; Sampath, S. *J. Colloid Interface Sci.* **2005**, *290*, 117.
(12) (a) Luo, J.; Maye, M. M.; Kariukia, N. N.; Wang, L.; Njoki, P.; Lin, Y.; Schadt, M.; Naslund, H. R.; Zhong, C. J. *Catal. Today* **2005**, *99*, 291. (b) Luo, J.; Maye, M. M.; Petkov, V.; Kariukia, N. N.; Wang, L.; Njoki, P.; Mott, D.; Lin, Y.; Zhong, C. J. *Chem. Mater.* **2005**, *17*, 3086.
(13) Nakanishia, M. *Appl. Surf. Sci.* **2005**, *241*, 209.
(14) (a) Gao, L.; Zhuang, J.; Nie, L.; Zhang, J.; Zhuang, Y.; Gu, N.; Wang, T.; Feng, J.; Yang, D. L.; Perrett, S.; Yan, X. Y. *Nat. Nanotechnol.* **2007**, *2*, 577. (b) Asati, A.; Santra, S.; Kaittanis, C.; Nath, S.; Perez, J. M. *Angew. Chem., Int. Ed.* **2009**, *48*, 2308. (c) Dai, Z.; Liu, S.; Bao, J.; Ju, H. *Chem.—Eur. J.* **2009**, *15*, 4321. (d) Wei, H.; Wang, E. K. *Anal. Chem.* **2008**, *80*, 2250. (e) Gao, L.; Wu, J.; Lyle, S.; Zehr, K.; Cao, L.; Gao, D. *J. Phys. Chem. C* **2008**, *112*, 17357. (f) Yu, F.; Huang, Y.; Cole, A. J.; Yang, V. C. *Biomaterials* **2009**, *30*, 4716.
(15) (a) Kajita, M.; Hikosaka, K.; Iitsuka, M.; Kanayama, A.; Toshima, N.; Miyamoto, Y. *Free Radical Res.* **2007**, *41*, 615. (b) Kim, J.; Takahashi, M.; Shimizu, T.; Shirasawa, T.; Kajita, M.; Kanayama, A.; Miyamoto, Y. *Mech. Ageing Dev.* **2008**, *129*, 322. (c) Hamasaki, T.; Kashiwagi, T.; Imada, T.; Nakamichi, N.; Aramaki, S.; Toh, K.; Morisawa, S.; Shimakoshi, H.; Hisaeda, Y.; Shirahata, S. *Langmuir* **2008**, *24*, 7354. (d) Watanabe, A.; Kajita, M.; Kim, J.; Kanayama, A.; Takahashi, K.; Mashino, T.; Miyamoto, Y. *Nanotechnology* **2009**, *20*, 455105.
(16) He, W. W.; Wu, X. C.; Liu, J. B.; Zhang, K.; Chu, W. G.; Feng, L. L.; Hu, X. N.; Zhou, W. Y.; Xie, S. S. *J. Phys. Chem. C* **2009**, *113*, 10505.
(17) Michaels, A. M.; Nirmal, M.; Brus, L. E. *J. Am. Chem. Soc.* **1999**, *121*, 9932.
(18) (a) Xu, J. B.; Zhao, T. S.; Liang, Z. X. *J. Phys. Chem. C* **2008**, *112*, 17362. (b) Peng, Z. M.; Wu, J. B.; Yang, H. *Chem. Mater.* **2010**, *22*, 1098.
(19) Jana, N. R.; Gearheart, L.; Murphy, C. J. *Adv. Mater.* **2001**, *13*, 1389.

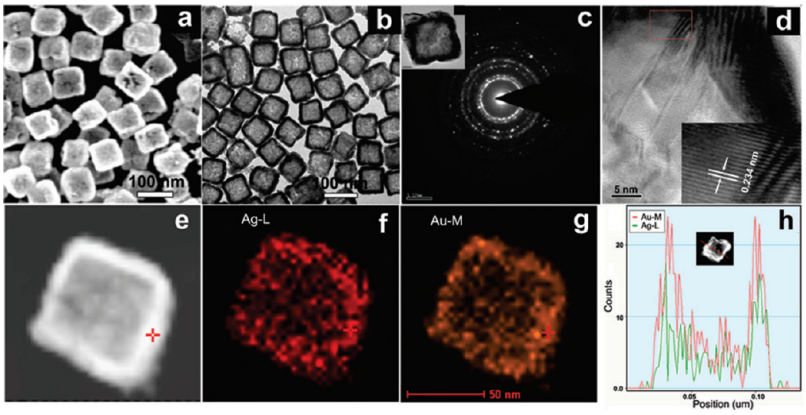

Figure 1. Typical (a) SEM and (b) TEM images of AgAu nanoboxes; (c) ED pattern of a single nanobox; (d) HRTEM image near the box wall; (e) STEM-HAADF image; (f, g) STEM-EDX element mappings of Ag and Au, respectively; and (h) cross-section composition line profiles of one nanobox. Inset in panel (d) shows an enlarged image of the red box noted in panel (d). Preparation conditions: 0.1 mM $AgNO_3$, 0.1 mM $AuCl_4^-$, and 0.4 mM AA.

(H_2SO_4/30% H_2O_2 = 7:3 v/v) and subjected to boiling for 30 min.

Synthesis of AgAu Nanoboxes. In a typical procedure for the synthesis of AgAu nanoboxes, 20 μL 10 mM $AuCl_4^-$ and 20 μL 10 mM $AgNO_3$ solution (molar ratio of 1/1) were mixed quickly with 2 mL of water. Immediately after mixing, 8 μL of 0.1 M AA was added, and the solution was shaken vigorously. The solution color changed to blue within < 30 s, indicating the formation of AuAg NPs. Afterward, 1 mL of 0.1 M CTAB was added to stabilize the NPs and keep them well-dispersed. 1 ml of the above solution was centrifuged (8000 rpm, 5 min) twice before further characterizations.

Synthesis of AgPd and AgPt Nanoparticles. To prepare AgPd NPs with a Ag/Pd ratio of 1/1, 200 μL of 2 mM $PdCl_4^{2-}$ and 40 μL of 10 mM $AgNO_3$ were mixed with 2 mL of 0.25 mM CTAB aqueous solution. Then, 0.1 M AA (AA/(Pd + Ag) = 2.0) was added. The solution immediately was shaken vigorously and then placed in a 30 °C water bath for 5 h. The color changed to dark brown, suggesting the formation of AgPd NPs. For AgPd NPs with different Ag/Pd ratios, the same procedure was applied with a fixed amount of $PdCl_4^{2-}$ and varied Ag ions. For OPD oxidation, AgPd NPs were prepared under the existence of 0.89 mM CTAB. In the case of AgPt NPs, $PtCl_4^{2-}$ solution is used to replace $PdCl_4^{2-}$ solution, and a dark gray color is observed for AgPt NPs. The as-prepared AgPd (AgPt) NPs were purified by centrifugation (12 000 rpm, 5 min) twice. The precipitates were redispersed in water for further characterizations and catalytic reactions.

Characterization. UV−vis−NIR absorption spectra were acquired with a Varian Model Cary 50 system, using a matched quartz cuvette with a path length of 1 cm. For scanning electron microscopy (SEM) (Hitachi Model S-4800) measurements, 10-μL concentrated samples were deposited dropwise onto a clean Si surface and dried at 100 °C in air. Transmission electron microscopy (TEM), high-resolution transmission electron microscopy (HRTEM), and selected-area electron diffraction were performed on Tecnai G^2 F20 U-TWIN. Scanning transmission electron microscopy (STEM) and energy-dispersive X-ray analysis (EDX) element mappings were conducted under a high-angle annular dark field (HAADF) mode from the same microscope. The samples for TEM analysis were prepared by adding drops of colloidal solutions onto standard holey carbon-coated copper grids. The grids were dried in air at room temperature.

The catalytic oxidation of OPD by alloy NPs, in the presence of H_2O_2, was performed as follows: 100 μL of 30% H_2O_2 and 10 μL of 0.1 M OPD (prepared freshly) were added to 3 mL of H_2O. Then, a certain amount of alloy NPs suspension was added into the above mixture. The oxidation reaction progress was monitored at 40 °C with 2-min intervals by recording the absorption spectra in a scanning kinetics mode.

Results and Discussion

Formation of AgAu Alloy Nanoboxes. The SEM image of AuAg NPs (Figure 1a) shows a cubic morphology with holes on the surface. The box shape is seen more clearly from the TEM image (Figure 1b), where the center portion of the nanobox is much lighter than the edge. The average size is 75.0 ± 5.0 nm in diameter, with a shell thickness of 9.6 ± 2.1 nm (averaged from 50 NPs in the TEM image). To investigate the crystal structure, the electron diffraction (ED) pattern and HRTEM are recorded and displayed in Figures 1c and 1d. The ED pattern shows that diffraction spots are superimposed on the rings, indicating the polycrystalline structure of the nanobox. In contrast, AgAu alloy nanocages, obtained by etching Ag nanocubes with Au^{3+} ions, have a single crystalline structure.[20] The lattice image near the box wall (Figure 1d, inset) reveals that the *d*-spacing of adjunct fringes is 0.234 nm, which is similar to the planar distance of Au[111] (0.235 nm) or Ag[111] (0.233 nm). To explore the elemental distribution of Ag and Au in the nanobox, STEM-EDX mapping measurements were performed (see Figures 1e−g). The element mappings show that Ag and Au are homogeneously mixed in the nanobox, indicating the formation of an alloy. The line profiles of composition also verify the higher percentage of Au and Ag at the box wall (see Figure 1h).

The shape of AuAg NPs is highly dependent on the added Ag/Au molar ratio (see Figure S1 in the Supporting Information). In the absence of $AgNO_3$, pure Au NPs have irregular shapes with a solid structure (see Figure S1a in the Supporting Information). At lower Ag/Au ratio (0.2), starlike solid NPs dominate. Increasing the Ag/Au ratios from 0.4 to 0.8, nanoboxes begin to appear and increase in number. The uniform nanoboxes are

(20) Chen, J. Y.; McLellan, J. M.; Siekkinen, A.; Xiong, Y. J.; Li, Z. Y.; Xia, Y. N. *J. Am. Chem. Soc.* **2006**, *128*, 14776.

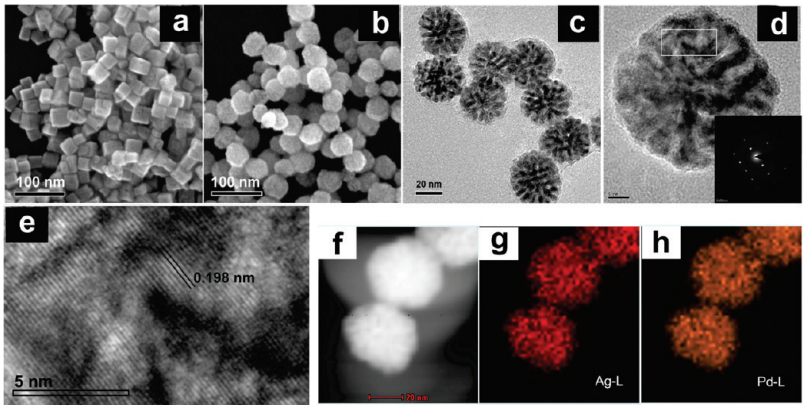

Figure 2. SEM image of (a) Pd nanocubes; (b) SEM, (c) TEM, and (d) HRTEM images of branched AgPd NCs. The inset in panel (d) is the corresponding ED pattern, and panel (e) is the enlarged image of the white box in panel (d). (f) STEM-HAADF image and STEM-EDS element mappings (for (g) Ag and (h) Pd) of AgPd NCs prepared at a Ag/Pd ratio of 1/1.

obtained at an Ag/Au ratio of 1/1. Broken nanoboxes are the predominant morphology at an Ag/Au ratio of 1.5. Therefore, the formation of AgAu nanoboxes is critically related to the involvement of Ag. Previously, the synthesis of cubic AgAu alloy nanocages was mainly demonstrated via the displacement reaction between Ag nanocubes with Au ions.[20] In our case, we believe that a similar mechanism works, although the sacrificial templates are AgAu nanoalloys with a higher Ag percentage. The formation of nanobox is determined by two competitive growth processes: the formation of Au atoms via the direct reduction by AA and via the displacement reaction with AgAu nanoalloys. Without Au ions, Ag ions cannot be reduced by AA at the employed conditions. In contrast, without Ag ions, solid Au NPs form. This suggests that Au ions are first reduced by AA and form the initial nuclei. Then, Au and Ag ions are co-reduced at the nuclei and lead to the growth of NPs. At lower Ag/Au ratios, Au deposits faster than Ag, and the obtained nanoalloys have a higher percentage of Au. At higher Ag/Au ratios, the scenario is different. Ag grows faster than Au, leading to the nanoalloys with a higher Ag percentage. Such alloys are known to have a large electrochemical driving force to reduce Au^{3+} ions via the displacement reaction. This opens the path of Au deposition via the displacement reaction and finally leads to the formation of the nanobox. At fixed Au ions (fixed nuclei density), a higher Ag/Au ratio results in a bigger alloy NP with a higher Ag percentage. After the displacement reaction, there are not enough Au atoms available to form a compact nanobox. Therefore, at an Ag/Au ratio of 1.5/1, mainly broken nanoboxes are found (see Figure S1g in the Supporting Information). For the nanobox prepared with an Au/Ag ion ratio of 1/1, the obtained Au/Ag atom ratio via the EDX analysis is ca. 1.9/1. This gives additional evidence that partial Au ions are reduced via the displacement reaction. The concentration of $AuCl_4^-$ and $AgNO_3$ also influences the morphology (see Figure S2 in the Supporting Information). The size of nanoboxes can be tuned by changing the reactant concentrations. At concentrations of >0.25 mM, starlike structures begin to appear. Apart from the Au/Ag ratio, the existence of CTAB changes the final morphology greatly. In the presence of CTAB (0.25 mM), instead of hollow structures, solid NPs form (see Figure S3 in the Supporting Information). They show an absorbance at ~550 nm (see Figure S4a in the Supporting Information). Instead, AuAg nanoboxes demonstrate a strong absorbance at 670 nm (see Figure S4b in the Supporting Information). In the presence of CTAB, a CTAB$-Ag^+$ complex forms. It greatly reduces the standard redox potential of Ag ions, for example, from +0.799 V for Ag^+/Ag to +0.07 V in the case of AgBr/Ag.[21] Thus, the reduction of Ag ions is greatly restricted and mainly solid Au NPs form.

Formation of Branched AgPd Alloy Nanocrystals (NCs). In the combination of Ag and Pd, involvement of Ag also impacts the morphology greatly, as shown later in Figure 3. In the absence of $AgNO_3$, Pd NPs with a cubic shape form through the direct reduction of Pd(II) ions by AA under 0.25 mM CTAB (Figure 2a). The addition of Ag induces the formation of spherical NPs with a branched structure at a Ag/Pd ratio of 1/1 or lower (see Figures S5b and S5c in the Supporting Information). The branched structure becomes more condensed at Ag/Pd ratios of 3 and 5 (see Figures S5d and 5e in the Supporting Information). To understand the branched structure better, the NPs obtained at a Ag/Pd ratio of 1/1 are further characterized (see Figure 2b and c). The particle size is 46.0 ± 5.9 nm in diameter, averaged from 73 NPs (TEM images). The coexistence of silver and palladium in the AgPd NPs is demonstrated by EDX (data not shown here). To investigate the crystal structure, the HRTEM image and ED pattern were captured (see Figure 2d and inset). The diffraction spots of the single AgPd NP indicate a single crystalline structure. The enlarged HRTEM image shows well-defined two-dimensional lattice planes (see Figure 2e). The calculated lattice spacing of the [002] plane is 0.198 nm, which is between that of pure Ag and Pd, suggesting the formation of an alloyed NC. Element mapping analysis further

(21) (a) Chen, S. H.; Carroll, D. L. *J. Phys. Chem. B* **2004**, *108*, 5500. (b) Niidome, Y.; Nakamura, Y.; Honda, K.; Akiyama, Y.; Nishioka, K.; Kawasaki, H.; Nakashima, N. *Chem. Commun.* **2009**, 1754.

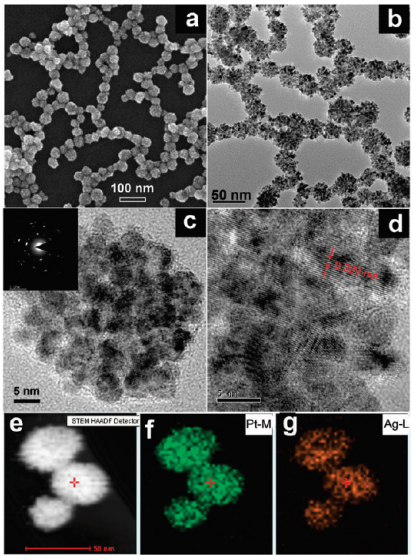

Figure 3. (a) SEM image and (b) TEM image of porous AgPt NSs. (c) HRTEM image (and corresponding ED pattern) and (d) lattice image from a single AgPt NS. (e) STEM-HAADF image and STEM-EDX element mappings for (f) Pt and (g) Ag of AgPt NSs with an added Ag/Pt ratio of 1/1.

verifies this conclusion (see Figures 2f−h). Ag and Pd are homogeneously distributed over the entire particle. The alloy composition measured by EDX is $Ag_{0.44}Pd_{0.56}$, which is similar to the added Ag/Pd ratio (1/1). The formation of AgPd nanoalloys is also verified from UV−vis-NIR absorption spectra (see Figure S6 in the Supporting Information). As expected, pure Pd NCs show a featureless absorption spectrum from 900 nm to 300 nm, with a gradual increase in absorption intensity toward shorter wavelengths. In addition, no discrete SPR absorption band is observed. When the Ag/Pd ratio was increased from 1 to 3, similar to Pd NCs, no SPR band appeared. At a Ag/Pd ratio of 4, a very broad SPR band starts from longer wavelengths (ca. 900 nm) and reaches the maximum at 366 nm. At a Ag/Pd ratio of 5, the SPR maximum shifts to 400 nm and becomes much stronger. Because of the strong damping of Pd, nanoalloys at lower Ag/Pd ratios do not show any observable SPR features. At higher Ag/Pd ratios, Ag becomes dominant. The SPR band appears and shifts to the SPR position of Ag with increasing Ag percentage, accompanied by an enhancement in SPR intensity.

Formation of Porous AgPt Alloy Nanospheres (NSs). Similarly, this approach can be extended to the synthesis of AgPt NPs. Notice that both Pt and Ag monometallic NPs cannot be formed under this condition. Figures 3a and 3b show the SEM and TEM images of the AgPt NPs. A spherical shape from the SEM image and a porous structure from the TEM image can be observed and are evident. The porous AgPt NPs have an average diameter of 37.5 ± 6.0 nm (calculated from 72 NPs). The HRTEM image indicates that a single NP is composed of small NCs (< 5 nm in diameter). The corresponding ED pattern shows rings that consist of diffraction spots, indicating a polycrystalline structure for the single AgPt NS (see Figure 3c). The calculated lattice spacing of the [111] plane is 0.229 nm (see Figure 3d), which lies between that of pure Pt and Ag, verifying the formation of an alloy. In a single AgPt NP, small NCs exhibit well-defined two-dimensional (2-D) lattice images, indicating that each small NC has a single crystalline structure. Moreover, different small NCs have different spatial orientations, thus leading to the polycrystalline structure of the entire NP. The AgPt NPs are actually spherical aggregates of the small AgPt alloy NCs. Therefore, we call them AgPt NSs. The STEM-EDX mappings (Figures 3e−g) show that Ag and Pt coexist and are well-dispersed in the nanosphere (NS), in agreement with HRTEM results. The alloy composition measured by EDX is $Ag_{0.45}Pt_{0.55}$, which is similar to the added Ag/Pt ratio (1/1). In the absence of $AgNO_3$, Pt NPs cannot be formed, possibly because of the lack of nuclei. It has been demonstrated that Ag clusters containing as few as four atoms could promote the deposition of Pt on the low-index planes.[22] Hence, Ag may play an auxiliary role in triggering nuclei formation. The single-crystalline nature of each small alloy NC supports this conclusion.

The Role of CTAB Molecules. CTAB molecules are critical to the formation of branched AgPd NCs and porous AgPt NSs. Figure 4 presents morphologies of AgPd NPs obtained at different CTAB concentrations. Solid AgPd NCs with a spherical-like structure are obtained in the absence of CTAB (Figure 4a). Similar to AgPd NCs synthesized under 0.25 mM CTAB, they remain a porous structure at 0.89 mM CTAB with a slightly decreased particle size. Increasing the CTAB concentration to 8.9 mM and above, solid AgPd NCs with octahedral, triangular, and multitwinned structures are formed. As discussed for AgAu nanoalloys, the existence of CTAB limits the reduction of Ag ions. This limitation also happens for the AgPd system (Figure 4f). Increasing the CTAB concentration, the Ag/Pd ratio of the nanoalloy from EDX analysis decreases from 0.75 (0.89 mM CTAB) to 0.35 (30 mM CTAB). In contrast, at these Ag/Pd ratios, branched AgPd NCs form at a CTAB concentration of 0.89 mM (see Figure S5 in the Supporting Information). Therefore, it is CTAB rather than the Ag/Pd ratio that plays a dominant role in morphology control. Apart from restraining Ag reduction, CTAB also greatly influences the reaction rate. At 0.25 mM CTAB, the reaction is completed within 3−4 h, whereas it takes 24 h to be finished at 30 mM CTAB. According to theoretical calculations, faster reaction rates due to a higher driving force can lead to a continuous growth mode, producing a porous structure, while slower reaction rates due to a lower driving force can result in a layer-by-layer growth mode, which generates anisotropic nanostructures.[23] To obtain more insight into the reaction kinetics, the effect of reaction temperature was explored (see Figure S7 in the Supporting Information). Temperature

(22) Teng, X. W.; Yang, H. *Nano Lett.* **2005**, *5*, 885.
(23) Viswanath, B.; Kundu, P.; Halder, A.; Ravishankar, N. *J. Phys. Chem. C* **2009**, *113*, 16866.

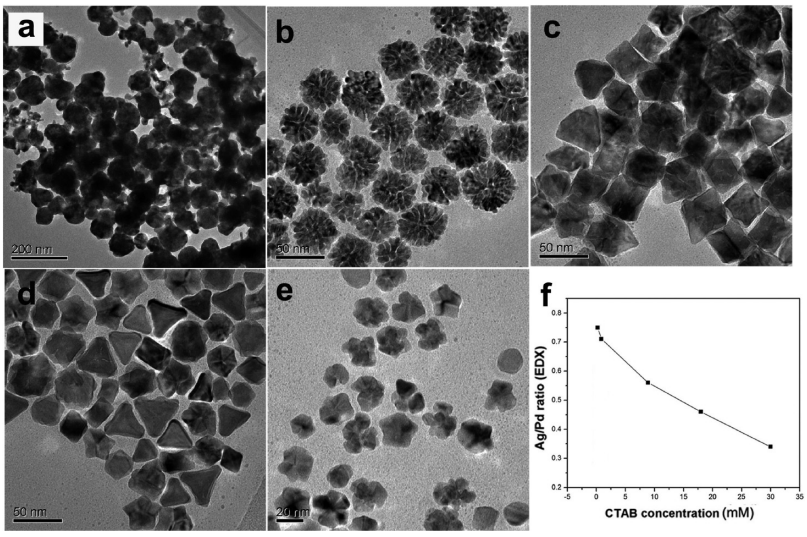

Figure 4. TEM images of AgPd NCs obtained at an added Ag/Pd ratio of 1/1 and different CTAB concentrations: (a) 0 mM, (b) 0.89 mM, (c) 8.9 mM, (d) 18 mM, and (e) 30 mM. Panel (f) shows the effect of CTAB concentration on the actual Ag/Pd ratio in AgPd NCs, as measured by EDX.

seems to play a very complex role. The size of alloy NPs obviously decreases as the temperature increases. Hence, temperature not only influences the growth kinetics but also the nucleation process. At 0.89 mM CTAB, the number of branched NCs decreases with increasing temperature. At 8.9 mM CTAB, increasing the temperature does not lead to the conversion of solid NCs to branched structures. Herein, reaction kinetics is not the main factor in morphology control. The formation mechanism of the branched structure requires further investigation. The branched AgPd NCs are single-crystalline, whereas the porous AgPt NSs are polycrystalline. The difference is mainly related to the different miscibility between AgPt and AgPd. Ag and Pd are miscible, while Ag and Pt have a broad miscibility gap at < 900 K.[24] At particle sizes of < 5 nm, Pt and Ag can form an alloy. As shown in Figure 3, each small alloy NC is single-crystalline, supporting the miscibility of Ag and Pt at small sizes. To decrease the surface energy, they form large spheres via rapid aggregation, thus forming a polycrystalline structure. Figure S8 in the Supporting Information displays a HRTEM image of an AgPt particle formed in 0.25 mM CTAB. The reaction was terminated after 3 min. The fast Fourier transform (FFT) images of selected parts show different crystal orientations, indicating that the entire particle is an aggregate of small NCs. Taken together, by fine-tuning reaction parameters, alloy NPs with controlled morphology can be obtained.

Composition Dependence of Peroxidase-Like Activity for AgPd Nanocrystals. Recently, peroxidase-like activity has been reported for Fe_3O_4 NPs and sheetlike FeS nanostructures.[14] In our previous report, we found that $Au@Pt_xAg_{1-x}$ ($0.44 < x < 0.62$) alloy NRs show a composition dependence on the catalytic oxidation of OPD in the presence of H_2O_2.[9f] Therefore, it motivates us to explore the possibility of noble-metal NPs as a new candidate of artificial peroxidase. Here, we focus the investigation on AgPd NCs. Similar to HRP, they can quickly catalyze the oxidation of typical HRP substrates (TMB, OPD, and ABTS) (see Figure 5a), suggesting peroxidase-like activity. The AgPd NCs with different

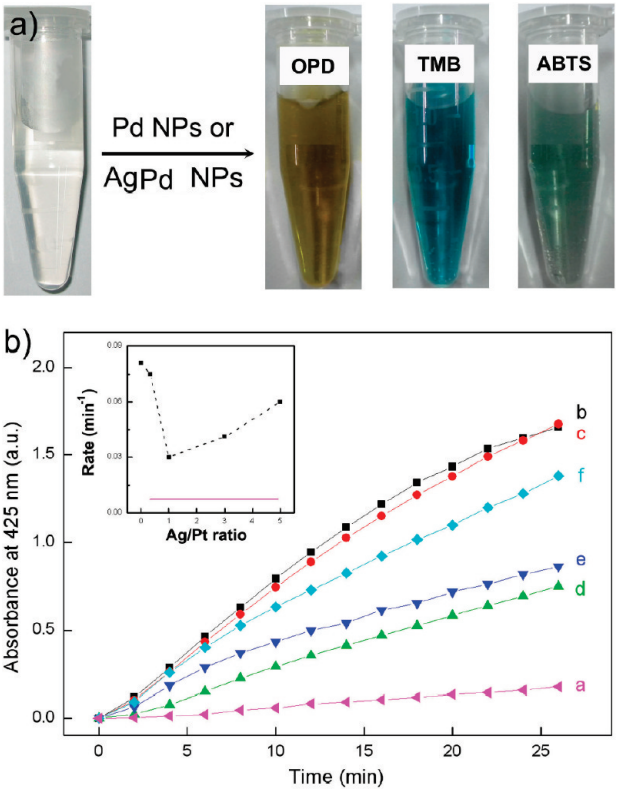

Figure 5. (a) Color evolutions of OPD, TMB, and ABTS oxidation catalyzed by Pd NCs or AgPd NCs. (b) Absorbance at 425 nm as a function of time after adding the same dosages of Pd NCs (curve b) and AgPd NCs with Ag/Pd ratios of 1/3 (curve c), 1/1 (curve d), 3/1 (curve e), and 5/1 (curve f). (Curve a represents the control experiment without catalyst.) Inset in panel (b) shows the the dependence of OPD oxidation rate on the Ag/Pd ratio. The purple line marks the value of the control experiment. Reaction conditions: 0.3 M H_2O_2, 0.3 mM OPD, and 26 μM Pd NCs or AgPd NCs (according to the concentration of Pd atoms) at 40 °C.

(24) Hansen, M.; Anderko, K.; *Consitution of Binary Alloys*; McGraw–Hill: New York, 1958.

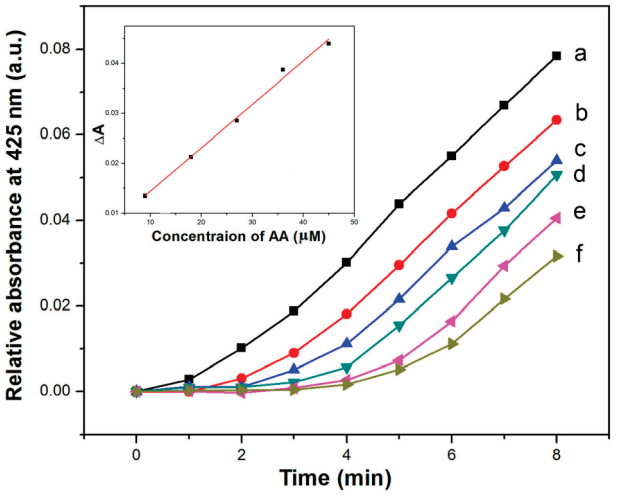

Figure 6. The absorbance evolution at 425 nm over time for OPD oxidation catalyzed by AgPd NCs with a Ag/Pd ratio of 1/3 without AA (curve a) and after addition of AA of 9 μM (curve b), 18 μM (curve c), 27 μM (curve d), 36 μM (curve e), and 45 μM (curve f). Inset shows the linear relationship between absorbance change at 6 min and concentration of AA, $\Delta A = A_0 - A_i$ (A_0 and A_i are the absorbance at 425 nm before and after addition of AA with a concentration of i, respectively). Reaction conditions: 0.3 mM OPD and 0.09 M H_2O_2 at T = 40 °C.

alloy compositions all demonstrate catalytic activity for OPD oxidation (see Figure 5 in the text and Figure S9 in the Supporting Information). The initial oxidation rates are evaluated by monitoring the absorbance increase of OPD oxidization product at 425 nm. Pd NCs has the highest catalytic activity, albeit with a solid structure (see Figure 5b). By forming AgPd nanoalloys with a Ag/Pd ratio of 0.33, the activity is reduced only slightly, possibly benefiting from the branched structure. The nanoalloys with a Ag/Pd ratio of 1 have the lowest activity. Increasing the Ag/Pd ratio to 3/1 and 5/1, a gradual enhancement in activity is observed (see Figures 5e and 5f). The initial reaction rate vs Ag/Pd ratio exhibits a "valley" shape. The variation in electronic structure due to alloying is believed to be responsible for the observed dependence. In addition, although alloying with Pd greatly enhances the stability of Ag, AgPd alloy NCs at higher Ag/Pd ratios are not stable enough in the presence of H_2O_2. They are partially oxidized to produce Ag^+ ions. For AgPd NCs with a Ag/Pd ratio of 3/1, ca. 27% of OPD molecules are oxidized by Ag^+ ions (see Figure S10A in the Supporting Information). In contrast, no leaching of Ag^+ ions is observed for AgPd alloy NCs at a Ag/Pd ratio of $\leq$1 (see Figure S10B in the Supporting Information). AgPt NSs (Ag/Pt = 1) and AgAu nanoboxes (Ag/Au = 1/2) also show catalytic activity for OPD oxidation (see Figures S9c and S9d in the Supporting Information). Our findings suggest a new type of candidate for peroxidase mimics.

Detection of Ascorbic Acid by Inhibiting the OPD Oxidation. Ascorbic acid is an essential nutrient and a well-known antioxidant that protects other important biomolecules against oxidation by many oxidants, especially reactive oxygen species (ROS). We find that the existence of AA can inhibit the oxidation of OPD by hydrogen peroxide (H_2O_2). The inhibiting effect is attributed to the competition oxidation of AA and OPD by H_2O_2. Figure 6a shows the absorbance increase at 425 nm with time. When AA is added, the absorbance increase at 425 nm is slowed. The inhibition ability is dependent on the concentration of AA (see Figures 6b–f). A higher concentration of AA leads to a stronger inhibition. Based on the inhibiting effect, a simple method is developed to detect AA. A nice linear relationship exists between the absorbance, and the concentration of AA and the limit of detection for AA is ca. 6.7 μM.

Conclusions

One facile and effective approach, based on the co-reduction of two metal ions by a weak reductant without seeding templates, is developed for the preparation of Ag-related bimetallic alloy nanoparticles (NPs) with hollow/porous structures. AgAu nanoboxes, branched AgPd NCs, and porous AgPt NSs are obtained. The surfactant CTAB molecules greatly affect the morphologies. This approach may be extended to prepare other bimetallic NPs. AgM alloy NPs with proper Ag/M ratios exhibit stable peroxidase-like activity. Furthermore, enzyme activity can be tailored by alloy composition, suggesting another effective way to tune the activity apart from size and shape. Because of their low costs, tunable composition and structure, and high stability, these novel bimetallic alloy NPs may represent a promising candidate of mimetic enzymes and will find a wide range of new applications, such as immunoassay, biocatalysis, and environmental monitoring.

Acknowledgment. The work was supported by National Natural Science Foundation of China (Grant No. 20773032) and the "973" National Key Basic Research Program of China (2006CB932602 and 2006CB705600).

Supporting Information Available: SEM images of AgAu NPs prepared under different Ag/Au ratios and different initial concentrations (Figures S1 and S2); TEM image of AgAu NPs prepared in the presence of CTAB (Figure S3); UV–vis–NIR absorption spectra of AgAu NPs (Figure S4); SEM images and UV–vis-NIR absorption spectra of AgPd NPs with different Ag/Pd ratios (Figures S5 and S6, respectively); effect of reaction temperature on morphology (Figure S7); HRTEM image of a single AgPt NS (Figure S8); the evolution of absorbance spectra of OPD oxidation over time (Figure S9); and effect of leaching on OPD oxidation (Figure S10). This material is available free of charge via the Internet at http://pubs.acs.org.